ENVIRONMENTAL RESEARCH
LETTERS

PURPOSE-LED PUBLISHING™

LETTER • OPEN ACCESS

Precipitation extremes projected to increase and to occur in different times of the year

To cite this article: Dario Treppiedi *et al* 2025 *Environ. Res. Lett.* **20** 014014

ENVIRONMENTAL RESEARCH
LETTERS

OPEN ACCESS

RECEIVED
14 September 2024

REVISED
14 November 2024

ACCEPTED FOR PUBLICATION
28 November 2024

PUBLISHED
9 December 2024

LETTER

Precipitation extremes projected to increase and to occur in different times of the year

Dario Treppiedi[1,*], **Gabriele Villarini**[2,3], **Jens Bender**[4] **and Leonardo Valerio Noto**[1]

[1] Dipartimento di Ingegneria, Università degli Studi di Palermo, Palermo, Italy
[2] Civil and Environmental Engineering, Princeton University, Princeton, NJ, United States of America
[3] High Meadows Environmental Institute, Princeton University, Princeton, NJ, United States of America
[4] Baden-Wuerttemberg Cooperative State University, Mosbach, Germany
[*] Author to whom any correspondence should be addressed.

E-mail: dario.treppiedi@unipa.it

Keywords: extreme precipitation, magnitude, seasonality, future changes, circular–linear bivariate modeling, circular statistics

Supplementary material for this article is available online

Abstract

There is high confidence that precipitation extremes are projected to become more frequent and severe and, to a lesser extent, that their seasonality may change. However, these precipitation characteristics are dealt with separately, without examining whether magnitude and seasonality are jointly projected to change. Here we assess how the seasonality and magnitude of precipitation extremes are jointly projected to change for different climate scenarios. We perform analyses at the global scale using nine global climate models and four different emission scenarios. We identify large areas of the globe where the magnitude of the extremes is expected to increase as the emissions increase; at the same time, large changes in the seasonality of these extremes are projected to impact regions mainly located in the tropical and sub-tropical areas. These changes could impact our response and mitigation efforts and our resilience against such phenomena in response to climate change.

1. Introduction

Extreme precipitation is becoming more intense and frequent, exacerbating known impacts and emphasizing new ones (IPCC 2021). Severe storms can directly affect agriculture, triggering a cascade of events that can induce crop failure, worsen poverty, starvation, and conflicts across the globe (Rosenzweig *et al* 2002, Raleigh and Kniveton 2012, Abiodun *et al* 2017, Organization 2018); they also pose a significant threat for public health, increasing the possibility of waterborne disease (Checkley *et al* 2000, Curriero *et al* 2001, Thomas *et al* 2006, Khan *et al* 2015). These effects are felt in terms of the global economy, especially for the high-income countries (Kotz *et al* 2022).

Therefore, it is no surprise that changes in the characteristics of precipitation extremes have been extensively investigated across different spatial and temporal scales (Westra *et al* 2014, Donat *et al* 2016, Fowler *et al* 2021, Seneviratne *et al* 2021, Du *et al* 2022). Compared to a large body of existing literature exploring the changes in the magnitude of extreme precipitation, a smaller number of studies have explored the changes in seasonality as their main focus (Kent *et al* 2015, Brönnimann *et al* 2018, Marelle *et al* 2018, Song *et al* 2018, 2020, Dong *et al* 2019). Moreover, apart from some works (e.g. Dhakal *et al* 2015, Wainwright *et al* 2021), the standard approach in modeling seasonality is to create seasonal or monthly blocks, not allowing this variable to be modeled continuously and potentially overlooking changes in its timing. Hence, our understanding of the projected changes in these events is predicated on the assumption that they will continue to occur in the same season (i.e. stationarity), and so is our management of the water resources and response to their impacts. Substantial shifts in the timing of the wet season can have large impacts on plants and vegetation, especially in semi-arid areas. Weltzin *et al* (2003) suggest that shifts in precipitation regimes may lead to severe impacts to ecosystem dynamics, even stronger than the increase in temperature driven

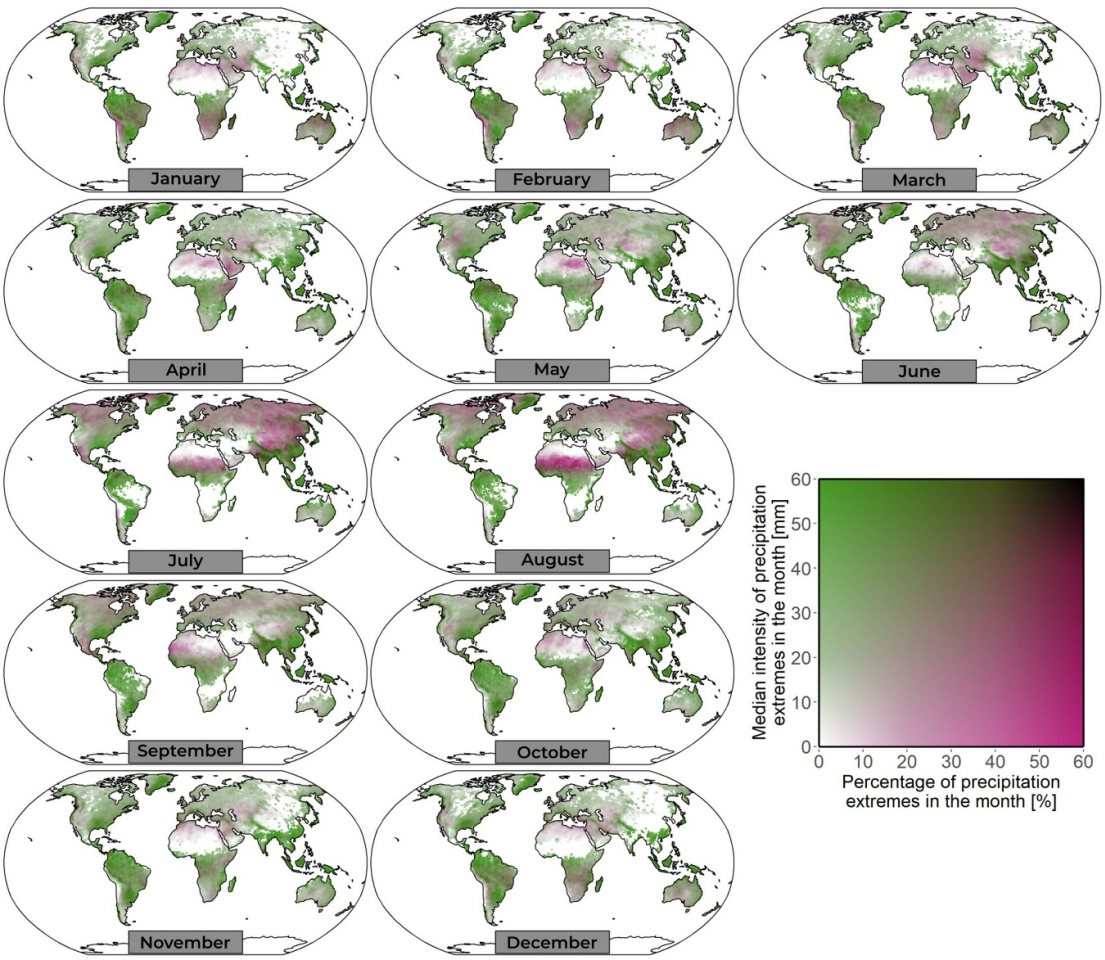

Figure 1. Bivariate representation of the monthly correlation between the percentage of daily precipitation values that exceed the 99th percentile of the grid cell distribution (i.e. precipitation extremes) and their median value at a global scale over the 1979–2014 period for the reference dataset (MSWEP-v2). The white-to-purple scale represents the percentage of extremes in the month, while the white-to-green one characterizes the magnitude of the median of the extremes in the month. Hence, the greener (more purple) the color, the greater (lower) the magnitude of the extreme precipitation in a given month, and at the same time, the lower (higher) the number of extremes that characterize it. Dark colors represent high percentages and high magnitudes of precipitation extremes, while totally white pixels indicate that no extremes occurred during the study period.

by CO_2. Ecosystems can be influenced by shifts in the onset of the rainy season, since this marks some fundamental moments in the biotic cycle (Feng *et al* 2013, Zeppel *et al* 2014). Potential changes in the timing of extreme precipitation are also important for storm water management and preparation against these events (Li *et al* 2021). All these impacts could be exacerbated if we consider that a shift in the timing of extreme precipitation may contribute, along with changes in soil moisture and snow processes, to alter the timing of flooding (Blöschl *et al* 2017, Wasko *et al* 2020, Kim and Villarini 2024).

How do we account for changes in precipitation magnitude and seasonality not in isolation, but rather within the same analysis framework? Despite the importance of this topic, there is no study that examines these two extreme precipitation characteristics jointly, except when seasons are pre-defined through blocks. Figure 1 highlights the monthly percentages of precipitation extremes (i.e. identified with respect to the 99th percentile of the all-day precipitation distribution) together with their magnitude (i.e. median value of the extremes exceeding the 99th percentile) based on a reference dataset (Beck *et al* 2019; section 2); for each month, we count the number of exceedances and compute their median value, highlighting how the extreme precipitation is distributed or concentrated during the year.

By analyzing the patterns from a univariate perspective, we can recognize areas without a dominant season, with large precipitation extremes that can occur throughout the year. This is the case for the southeastern United States, where large precipitation events can occur during almost any month due to extra-tropical cyclones, tropical cyclones, and mesoscale convective systems. South America, especially Argentina and Chile, is another such area. Extreme precipitation can occur throughout the year in equatorial Africa due to the Intertropical Convergence Zone (ITCZ), which determines the two

rainy seasons in the region (Nicholson 2018). Finally, the Mediterranean area and Central Europe exhibit a similar behavior, with extreme precipitation that can occur during the wet season from October to March but also during the boreal summer due to convective phenomena (Llasat *et al* 2021).

On the other side of the spectrum, some regions are characterized by a strong synchronism between the frequency and magnitude of extremes. For Russia or continental China, the highest values are concentrated in boreal summer (Fujinami *et al* 2016, Li and Ma 2018), primarily controlled by the variability in the subtropical Asia westerly jets, which increases moisture transport, creating favorable conditions for intense convection and precipitation (Xu *et al* 2022, Lei *et al* 2024). The strong synchronism is also the case for Saharan Africa, where most extremes occur between May and August, but with low intensity values. The Amazon Forest shows a bimodality in the extreme rainfall regime because of the seasonal migration of the ITCZ. Areas with a strong precipitation seasonality are also located in India, the Indochinese Peninsula and along the Chinese coast, with extremes concentrated between June and September due to the monsoon. For these areas, as well as for southern Africa and northern Australia in the austral summer, there is a high frequency of occurrence of extreme precipitation coupled with large intensities. For all these areas, there is a need for a joint analysis to better model the dependence between these two precipitation characteristics.

Therefore, the scope of this study is to jointly model the magnitude and seasonality of extreme precipitation at the global scale, and to examine how these two characteristics are projected to change under different scenarios.

2. Data and methods

2.1. Datasets

We use the Multi-Source Weighted-Ensemble Precipitation version 2 (MSWEP V2) (Beck *et al* 2019) as reference dataset during 1979–2014; it is global, derived by merging quality-controlled gauges, satellites, and reanalysis precipitation estimates, with a 0.1-degree spatial resolution and we aggregate it to the daily scale.

To assess future changes in precipitation characteristic, we use global climate models (GCMs) part of the Coupled Model Intercomparison Projects Phase 6 (CMIP6) (Eyring *et al* 2016). We focus on models with 100 km nominal resolution (∼1°) and with the historical and the future Shared Socio-economic Pathways (SSPs) scenarios (i.e. SSP1-2.6, SSP2-4.5, SSP3-7.0 and, SSP5-8.5), selecting nine GCMs (table S.1) and using the 'r1i1p1f1′ member (this selection is a tradeoff between computational expenses, and model resolution and ensemble size). The period for the historical experiment matches the one used for the reference (i.e. 1979–2014), while we select 2065–2100 for future scenarios. Since the reference data and GCM outputs have different spatial resolutions, we upscale the MSWEP to the GCMs resolution by means of bilinear interpolation.

For each pixel, we consider the 99th percentile of the whole daily precipitation distribution (i.e. considering both wet and dry days) as the threshold to detect extreme precipitation (Schär *et al* 2016).

2.2. Bivariate modeling of magnitude and seasonality of precipitation extremes

We propose a new statistical approach to derive potential changes in the magnitude and the seasonality of precipitation extremes, whose strength and occurrence are modeled using circular–linear bivariate copulae, $C(u,v)$, where u refers to the circular and v to the linear variable. The rainfall depth, h (mm), can be analyzed through standard linear statistics (i.e. it is a variable with a lower bound at zero), while the day within a year in which a given event occurs, d (day), needs to be analyzed through circular statistics because of its periodic nature (Cremers and Klugkist 2018). We use five different copulae derived from a linear combination and a rectangular patchwork of different Archimedean copulae (i.e. Clayton, Frank and Gumbel). For further details on the mathematical and statistical framework of copulas, see Hodel and Fieberg (2022) and the 'cylcop' (Hodel and Fieberg 2021) R package.

Considering the time series for each pixel and dataset (i.e. reference and CMIP6 GCMs), we use the Akaike information criterion (AIC) as performance metric to select the best copula. To verify if the GCMs can capture the statistical dependence between the two variables we use a bootstrap approach based on the AIC. We first generate 1000 random samples from the best copula selected for the reference data; for each sample, which has the same size as the original one, we recompute the AIC, allowing us to derive a reference AIC distribution for each pixel of the dataset. The reference best copula is then fitted to the extremes extracted from the historical experiment of the nine GCMs and the corresponding AIC values are computed. If these AIC values are between the 2.5 and the 97.5 percentiles of the reference AIC distribution, then there is not enough evidence to reject the null hypothesis that the GCM data are extracted from the same copula as the reference data. Hence, we consider this as a case in which the GCM can reproduce the statistical dependence in the reference data.

After this validation procedure, we apply the Rayleigh test (Pewsey *et al* 2013) to verify if there is uniformity in the seasonal component, namely if there is enough evidence to reject the null hypothesis

that the extreme precipitation values are uniformly distributed in the year.

Once this test is performed, we reapply the copula fitting procedure for each GCM and experiment. Indeed, even if we cannot reject the hypothesis that the precipitation extremes from the GCMs are extracted from the reference best copula, there may be one that better fits the data according to the AIC. After this step, we fit the marginal distributions. We consider the generalized Pareto distribution (GPD) as the marginal distribution for the rainfall depth, while we choose a mixture of N von Mises distributions (vMD) to model the marginal distribution of the circular variable. We evaluate the goodness-of-fit of the GPD distribution through the application of the Anderson–Darling test where the significance of the test is computed by means of a Monte Carlo approach (Choulakian and Stephens 2001). Since we do not know *a-priori* the optimal number of mixtures for the vMD, we test N ranging from one to four, and at the end we choose the model with the lowest Bayesian information criterion (Veatch and Villarini 2020, 2022). Figure S.1 shows a representation of the described procedure.

2.3. Assessing changes in the magnitude and seasonality of precipitation extremes

Once we model the bivariate dependence and the marginal distributions, we can quantify the variation in the characteristics of the extremes. For each experiment, we start generating one million random (u, v) pairs from the selected copula for every single pixel. Transforming these values to the original units through the marginal distributions, we can obtain a sample of rainfall depth, h, per each day, d, of the year. Hence, we compute the empirical cumulative distribution function conditioned to the date (ecdf($h|d$)), and we use its median value, $h_{50}(d)$, as a proxy for the extreme value that might occur on that day. An example is shown in figure S.2, in which the red line indicates the $h_{50}(d)$ and is superimposed onto the 2D density of the generated rainfall depth. Therefore, we consider the maximum of the daily median values as the reference rainfall depth (H_{50}) that may happen on a specific day ($D(H_{50})$) of the year according to the bivariate statistical structure derived from the data. Once these values are defined for each pixel (i) in each GCM (m) and experiment (hist and SSP), we quantify the future changes in the magnitude ($\Delta\bar{R}_{i,\,SSP}$) and seasonality ($\Delta\bar{S}_{i,\,\mathrm{SSP}}$) of precipitation extremes, compared to the historical experiments, by computing the following quantities:

$$\Delta\bar{R}_{i,\,\mathrm{SSP}} = 100 \cdot \frac{\bar{H}_{50_{i,\,\mathrm{SSP}}} - \bar{H}_{50_{i,\,\mathrm{hist}}}}{\bar{H}_{50_{i,\,\mathrm{hist}}}}\,[\%] \qquad (1)$$

$$\Delta\bar{S}_{i,\,\mathrm{SSP}} = \frac{\bar{D}(H_{50})_{i,\mathrm{hist}} - \bar{D}(H_{50})_{i,\mathrm{SSP}}}{30}\,[\mathrm{month}] \qquad (2)$$

where:

– $\bar{H}_{50_{i,\,\mathrm{SSP}}}$ and $\bar{H}_{50_{i,\,\mathrm{hist}}}$ represent the average of the H_{50} among the nine GCMs (m):

$$\bar{H}_{50\,i,\mathrm{SSP}} = \frac{1}{N}\sum_{m=1}^{N} H_{50i,\mathrm{SSP}_m}$$

$$\bar{H}_{50_{i,\,\mathrm{hist}}} = \frac{1}{N}\sum_{m=1}^{N} H_{50i,\mathrm{hist}_m}$$

– $\bar{D}(H_{50})_{i,\mathrm{SSP}}$ and $\bar{D}(H_{50})_{i,\mathrm{hist}}$ represent the circular mean of the $D(H_{50})$ among the nine GCMs (m):

$$\bar{D}(H_{50})_{i,\mathrm{SSP}} = \mathrm{circular.mean}\left(D(H_{50})_{i,\mathrm{SSP}_m}\right)$$

$$\bar{D}(H_{50})_{i,\mathrm{hist}} = \mathrm{circular.mean}\left(D(H_{50})_{i,\mathrm{hist}_m}\right).$$

For both the quantities we compute the average value among the GCMs to reduce the uncertainty associated with any individual model. Moreover, while in the case of $\bar{H}_{50_{i,\,\mathrm{SSP}}}$ and $\bar{D}(H_{50})_{i,\mathrm{hist}}$ it is possible to use the linear way to compute the average among the models, for $\bar{D}(H_{50})_{i,\mathrm{SSP}}$ and $\bar{D}(H_{50})_{i,\mathrm{hist}}$ it is important to compute the circular mean. In figure S.3 we show a schematic representation of the meaning of $\Delta\bar{R}_{i,\,\mathrm{SSP}}$ and $\Delta\bar{S}_{i,\,\mathrm{SSP}}$ on the circular–linear plane. Using equation (2), positive or negative shifts exceeding six months could be obtained; in all these cases, a forward (backward) shift that is higher than half a year is considered backward (forward) of the remaining months to complete a year.

3. Results and discussion

Based on the results in figure 1, the seasonality and magnitude of extreme precipitation exhibit regional variability; however, these two variables are also clearly connected, requiring them to be analyzed together rather than independently to get the full picture of how this hazard is projected to change. The first step is the development of bivariate models based on reference data (i.e. MSWEP-V2), which we use to examine whether the historical experiments from the nine GCMs can reproduce the observed bivariate structure of the precipitation extremes. The results from this validation procedure are presented in figure S.4, where we show the results based on the Intergovernmental Panel on Climate Change zones to provide a more regional view (Iturbide *et al* 2020). Globally, the GCMs can reproduce the observed results at almost all the pixels, reaching an average of 90% similarity within each region. Based on these results, the GCMs can capture the dependence in the precipitation extremes and can be used to provide insights about the projected changes in precipitation occurrence and magnitude.

We apply the Rayleigh test (significancy level 5%) to the reference dataset (a), the historical experiment (b) and the different emission scenarios (c)–(f) to verify the presence of uniformity in the seasonal variable (figure S.5). Since we consider an ensemble of nine GCMs, we stratify this information based on the number of GCMs that agree on uniformity. By comparing panels (a) and (b), we note that the areas in the historical experiment where the seasonal distribution is uniform across multiple models mostly match the uniform areas in the reference dataset. This is particularly true for the central and eastern United States, part of the South America, Spain, Indonesia and the area between Russia and Kazakhstan. There are also areas where uniformity is captured but by fewer models (e.g. Southern Australia) or part of the globe where it is overestimated (e.g. Eastern Europe and Northern and Central Africa). These areas correspond to those empirically identified from figure 1, namely all the ones that are characterized by different weather systems responsible for precipitation extremes. Moving to the future scenarios and, particularly, from SSP1-2.6 (i.e. panel (c)) to SSP5-8.5 (i.e. panel (f)), an expansion of these areas is particularly evident in Europe and the western part of Asia. Since these results translate into a weak seasonal dependence of extreme precipitation, we exclude these areas from the analyses below. Moreover, to be conservative, we exclude areas where at least one model identifies a uniform behavior of the seasonal component.

As reference quantity, we consider the maximum median value during a year as a proxy for the reference precipitation depth (H_{50}) that may occur on a specific day ($D(H_{50})$); by computing these quantities during the historical period (1979–2014) and into the future (2065–2100), we can quantify the precipitation changes in terms of magnitude ($\Delta\bar{R}$) and seasonality ($\Delta\bar{S}$) (figures S.2 and S.3). Figure 2 shows the projected changes in the characteristics of the extreme precipitation for the 2065–2100 period with respect to the historical baseline (i.e. 1979–2014) across the four different SSPs at the global scale. To present the results in a concise yet clear way, we have developed a bivariate continuous circular palette to display the changes in seasonality $\Delta\bar{S}$ (i.e. change in color) and the changes in magnitude $\Delta\bar{R}$ (i.e. change in brightness). Positive (negative) percentages for $\Delta\bar{R}$ indicate an increase (decrease) in the intensity of future extremes compared to the past. Related to the $\Delta\bar{S}$, positive (negative) values indicate a backward (forward) shift in seasonality. Figure S.6 presents the same results as figure 2 but uses a discretized representation of both $\Delta\bar{S}$ and $\Delta\bar{R}$.

Additionally, figure 3 shows a decoupled perspective of figure 2, namely the circular densities for $\Delta\bar{S}$ (panel (a)) and the linear ECDFs for $\Delta\bar{R}$ (panel (b)), which are useful to quantify their entities in each scenario.

For the areas without a uniform seasonality, our results suggest that climate change is expected to make precipitation extremes more intense compared to the past, consistent with previous studies (Zhang and Villarini 2017, Wu *et al* 2019, Chen and Sun 2021, Thackeray *et al* 2022). However, the changes in the magnitude are particularly tied to the emission scenario, moving from an increment that ranges from 0% to 40% in the case of the SSP1-2.6, to values up to 60%–70% for the highest emission scenario (figure 3(a)). The areas that are expected to experience the largest increases are mainly located in India and the area contiguous to the Bay of Bengal, pointing to a strengthening of the monsoon in the future (Menon *et al* 2013, Katzenberger *et al* 2021). Similar changes in magnitude are projected for the sub-Saharan Africa (see also Diem *et al* 2019, Jiang *et al* 2021), especially in the central and eastern Sahel region, associated with a fast response to climate change due to the enhanced radiative warming over land (Monerie *et al* 2021). We also decompose the global signals in the tropical, sub-tropical and temperate areas (figure S.7). The tropical regions exhibit the largest values of $\Delta\bar{R}$, especially under the high-emission scenarios (i.e. SSP3-7.0 and SSP5-8.5) (Chadwick *et al* 2016), pointing to the importance of climate policies in limiting the impacts of climate change. These increases are lower moving from the tropical regions to the subtropics (Lehmann *et al* 2015) and this reduction is even more evident when compared with the temperate areas. However, these changes in the extremes' magnitude are always positive, and might lead to even larger impacts considering that they are projected to occur in the upper tail of the precipitation distribution, jeopardizing the reliability of the infrastructures designed in the past (Nissen and Ulbrich 2017).

The results so far are just one side of the coin, with the potential changes in the time of the year in which these events occur representing the other one. There are large areas of the world exhibiting a temporal shift in the $D(H_{50})$ including South America, Africa, India, China and Indochinese Peninsula (figure 2). These findings are generally consistent regardless of the SSPs considered, even though there are asymmetries moving from SSP1-2.6 and SSP2-4.5 (i.e. the scatterplots are relatively symmetric around the no-change value) to SSP3-7.0 and SSP5-8.5 (i.e. there is a shift towards negative values). These asymmetries related to the emission scenarios are more evident when observing the density lines in figure 3(b). While for SSP1-2.6 80% of the density lies between $\sim\pm1.2$ months (i.e. the area between the green triangles in figure 3(b)), for SSP3-7.0 and SSP5-8.5 we observe an expansion of the tails of the distributions, especially the one related to a forward shift (i.e. negative $\Delta\bar{S}$) in the seasonality of extremes, reaching two months of change. Not only the tails, but also the

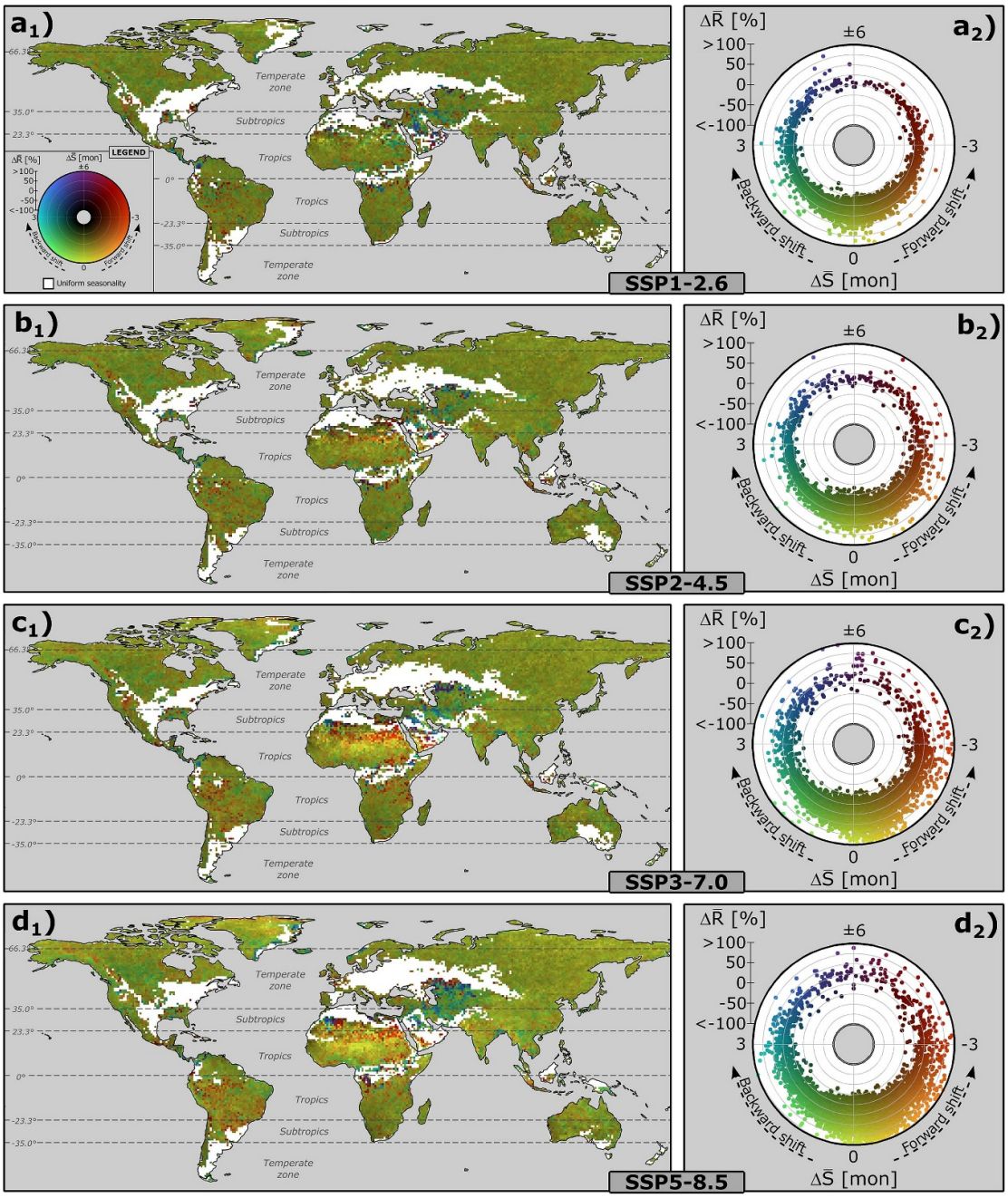

Figure 2. Average projected changes in the characteristics of the extreme precipitation for the 2065–2100 period with respect to the historical baseline (i.e. 1979–2014) under four emission scenarios (i.e. panels (a)–(d)). The bivariate circular palette is used to concurrently display the shift in the seasonality (i.e. $\Delta\bar{S}$ change in color) and the changes in the magnitude (i.e. $\Delta\bar{R}$ change in brightness). Positive (negative) percentages for the $\Delta\bar{R}$ indicate an increase (decrease) in the intensity of the future extremes compared to the past, while positive (negative) values for the $\Delta\bar{S}$ indicate a backward (forward) potential shift in the seasonality. Panels (a1), (b1), (c1) and (d1) show the spatial distribution of these changes, while the scatterplots (i.e. panels (a2), (b2), (c2) and (d2)) show where the pixel values are located within the bivariate circular plane.

median value tends to follow this drift toward positive $\Delta\bar{S}$ values, passing from no-change for SSP1-2.6 to 4 days for SSP3-7.0 and SSP5-8.5 (see table S.2 for their numerical values). From a physical point of view, this forward shift (i.e. extreme precipitation occurring later in the season) might be the result of a seasonal delay in the precipitation annual cycle, especially observed in the tropics (Biasutti and Sobel 2009, Dunning *et al* 2018, Song *et al* 2023). This delay was explained in terms of different mechanisms, including the cross-equatorial energy transport, which is mostly associated with the increased latent energy demand during the hemisphere's seasonal warming period (Song *et al* 2018), and a reduced availability of moisture at the beginning of the rainy season, related to an enhanced convective barrier mechanism (Seth *et al* 2011). For further details, one can consult Song *et al* (2023). The changes

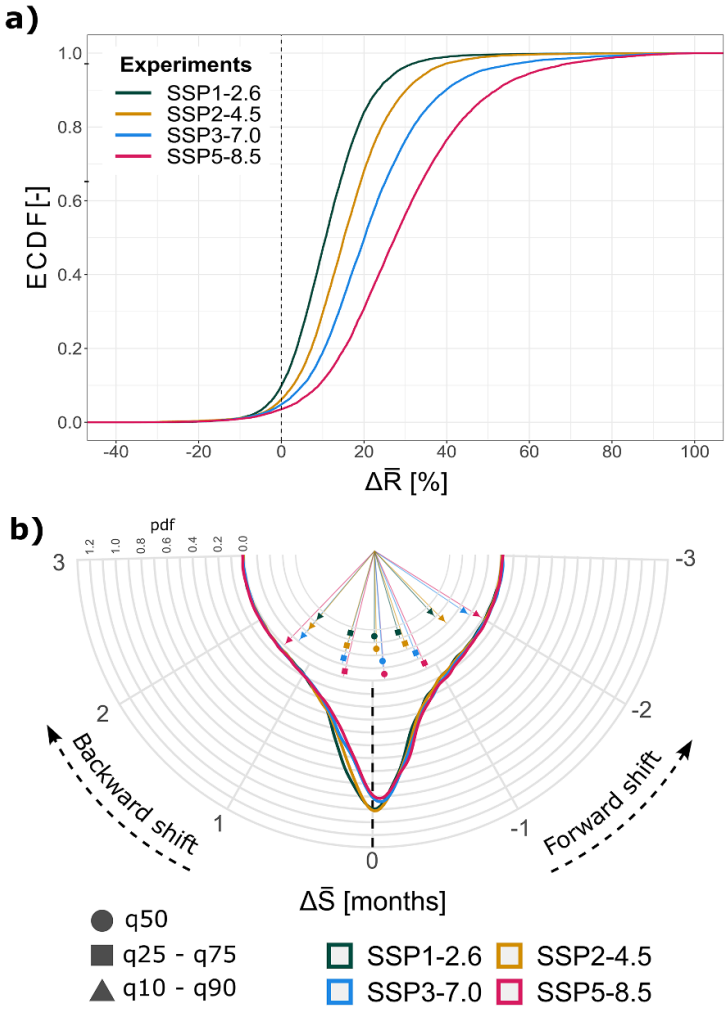

Figure 3. Decoupled average projected changes in the magnitude (panel (a)) and seasonality (panel (b)) of the extreme precipitation for the 2065–2100 period with respect to the historical baseline (i.e. 1979–2014) under four emission scenarios (i.e. colors). Panel a shows the empirical cumulative distribution function (ECDFs) for the $\Delta\bar{R}$ at different scenarios. Panel (b) shows the circular density distributions for the $\Delta\bar{S}$ at different scenarios. The circles, squares and triangles represent the values of some percentiles (i.e. 10th, 25th, 50th, 75th and 90th) for $\Delta\bar{S}$.

in seasonality are particularly evident across the Amazon Forest and southeastern Brazil, where there are shifts ranging from ∼15 d up to 2 months later in the season, larger than what was shown in Marelle *et al* (2018) (possibly because of different methodologies and model resolution); one possible explanation for our results is the potential impact of climate change in the seasonal precipitation related to El Niño Southern Oscillation (Grimm 2011). Focusing on the African continent, the central and the western part of the Saharan region seems to exhibit the largest changes in $\Delta\bar{S}$. The Sahel region is also characterized by large seasonal changes that can reach two-month delays. For both the Sahara and Sahel regions, there is a clear dependence on radiative forcing, with a clear transition from SSP1-2.6, where the signals are almost indistinguishable, to SSP3-7.0 and SSP5-8.5, which are characterized by the highest changes in the timing of extreme precipitation. Finally, the sub-equatorial Africa exhibits a behavior similar to South America, with the precipitation extremes that tend to occur later than the current timing. While the general tendency is towards extremes to occur later in the year, there are locations like Thailand, the area contiguous to the Bay of Bengal, and Philippines, where these phenomena are expected to occur earlier (Marelle *et al* 2018, Ha *et al* 2020) (i.e. teal green and bluish pixels in figure 2). The areas to the south and east of the Caspian Sea exhibit the most spatially widespread backward shift in seasonality, possibly driven by the projected anomalies in temperatures (Zarrin *et al* 2021), leading to prolonged hot seasons and alteration in the extreme precipitation temporal patterns. We also stratified the $\Delta\bar{S}$ for the tropics, sub-tropics, and temperate zones (figure S.8) with the tropical areas exhibiting the largest changes in the shape of the distribution, with a large expansion of the tail related to positive shifts, especially under the SSP3-7.0 and SSP5-8.5. We also observe a drift toward positive $\Delta\bar{S}$ values for the medians, with delays up

to two weeks for SSP3-7.0 and SSP5-8.5 (table S.2). Similar expansions are evident for the sub-tropics, although the distributions are in this case more symmetrical with respect to the no-change value and characterized by lower variability. Finally, this variability is even smaller when looking at the densities related to the temperate areas, although the effect of the increased greenhouse gas emission is present. These results underscore the importance of global climate policies, which are needed to limit as much as possible the effects of climate change.

4. Conclusions

We have analyzed the projected changes in the magnitude and seasonality of precipitation extremes, introducing a new approach based on circular–linear copulae. Our findings point not only to an increase in the magnitude of these phenomena, but also to changes in their seasonality in some regions. In particular, we exclude all the areas where precipitation extremes are evenly distributed throughout the year since different weather systems can be considered responsible for their genesis. However, long-term climate changes may also modify their timing and patterns, and so future developments will be devoted to also including these areas and quantifying the potential impacts across different sectors and spheres of our lives. With this novel methodology, future applications might also analyze different variables, also in the compound event framework, and how changes in the seasonality and magnitude of extreme precipitation events are captured when using different fixed or percentile-based thresholds.

By using a bivariate circular–linear model we can highlight that there are potentially large changes in when extremes can be expected, especially for high emission scenarios. We show that there could be an overall delay in the extreme rainfall season in various regions of the globe, especially in the tropics. However, there are also areas characterized by patterns where an advance in the seasonality is expected. This highlights the importance of conducting studies at a regional level to better understand these dynamics. We believe that these findings point to the need to develop mitigation and adaptation strategies that are flexible to account for the occurrence of extremes for times of the year during which we would not historically consider them likely to happen. Moreover, based on the SSP projections, the intensity of the precipitation extremes is expected to be exacerbated from SSP1-2.6 to SSP5-8.5, emphasizing the importance that actual policies and behaviors could have in addressing future climate change issues. Joint changes in the magnitude and timing of precipitation extremes can lead to significant and catastrophic impacts, such as increasing flood risk, altering water resources planning and stressing the agricultural systems. These changes can trigger ecosystem disruptions, affect infrastructure resilience, and complicate disaster management efforts. Finally, these results point to the need to consider the characteristics of precipitation extremes in a more holistic way, accounting for their potential interdependencies.

Data availability statement

The data that support the findings of this study are openly available at the following URL/DOI: www.gloh2o.org/mswep/;https://esgf-node.llnl.gov/projects/cmip6/.

Acknowledgments

Leonardo V Noto acknowledges financial support for Dario Treppiedi provided by Autorità di Bacino del Distretto Idrografico della Sicilia.

ORCID iDs

Dario Treppiedi https://orcid.org/0000-0002-1359-1650
Gabriele Villarini https://orcid.org/0000-0001-9566-2370
Jens Bender https://orcid.org/0009-0008-7588-6412

References

Abiodun B J, Adegoke J, Abatan A A, Ibe C A, Egbebiyi T S, Engelbrecht F and Pinto I 2017 Potential impacts of climate change on extreme precipitation over four African coastal cities *Clim. Change* **143** 399–413

Beck H E, Wood E F, Pan M, Fisher C K, Miralles D G, Van Dijk A I J M, Mcvicar T R and Adler R F 2019 MSWEP V2 global 3-hourly 0.1° precipitation: methodology and quantitative assessment *Bull. Am. Meteorol. Soc.* **100** 473–500

Biasutti M and Sobel A H 2009 Delayed Sahel rainfall and global seasonal cycle in a warmer climate *Geophys. Res. Lett.* **36** L23707

Blöschl G, Hall J, Parajka J, Perdigão R A, Merz B, Arheimer B, Aronica G T, Bilibashi A, Bonacci O and Borga M 2017 Changing climate shifts timing of European floods *Science* **357** 588–90

Brönnimann S, Rajczak J, Fischer E M, Raible C C, Rohrer M and Schär C 2018 Changing seasonality of moderate and extreme precipitation events in the Alps *Nat. Hazards Earth Syst. Sci.* **18** 2047–56

Chadwick R, Good P, Martin G and Rowell D P 2016 Large rainfall changes consistently projected over substantial areas of tropical land *Nat. Clim. Change* **6** 177–81

Checkley W, Epstein L D, Gilman R H, Figueroa D, Cama R I, Patz J A and Black R E 2000 Effects of EI Niño and ambient temperature on hospital admissions for diarrhoeal diseases in Peruvian children *Lancet* **355** 442–50

Chen H and Sun J 2021 Significant increase of the global population exposure to increased precipitation extremes in the future *Earth's Future* **9** e2020EF001941

Choulakian V and Stephens M A 2001 Goodness-of-fit tests for the generalized Pareto distribution *Technometrics* **43** 478–84

Cremers J and Klugkist I 2018 One direction? A tutorial for circular data analysis using R with examples in cognitive psychology *Front. Psychol.* **9** 2040

Curriero F C, Patz J A, Rose J B and Lele S 2001 The association between extreme precipitation and waterborne disease

outbreaks in the United States, 1948–1994 *Am. J. Public Health* **91** 1194–9
Dhakal N, Jain S, Gray A, Dandy M and Stancioff E 2015 Nonstationarity in seasonality of extreme precipitation: a nonparametric circular statistical approach and its application *Water Resour. Res.* **51** 4499–515
Diem J E, Konecky B L, Salerno J and Hartter J 2019 Is equatorial Africa getting wetter or drier? Insights from an evaluation of long-term, satellite-based rainfall estimates for western Uganda *Int. J. Climatol.* **39** 3334–47
Donat M G, Lowry A L, Alexander L V, O'Gorman P A and Maher N 2016 More extreme precipitation in the world's dry and wet regions *Nat. Clim. Change* **6** 508–13
Dong L, Leung L R, Lu J and Gao Y 2019 Contributions of extreme and non-extreme precipitation to California precipitation seasonality changes under warming *Geophys. Res. Lett.* **46** 13470–8
Du H *et al* 2022 Extreme precipitation on consecutive days occurs more often in a warming climate *Bull. Am. Meteorol. Soc.* **103** E1130–45
Dunning C M, Black E and Allan R P 2018 Later wet seasons with more intense rainfall over Africa under future climate change *J. Clim.* **31** 9719–38
Eyring V, Bony S, Meehl G A, Senior C A, Stevens B, Stouffer R J and Taylor K E 2016 Overview of the coupled model intercomparison project phase 6 (CMIP6) experimental design and organization *Geosci. Model Dev.* **9** 1937–58
Feng X, Porporato A and Rodriguez-Iturbe I 2013 Changes in rainfall seasonality in the tropics *Nat. Clim. Change* **3** 811–5
Fowler H J, Lenderink G, Prein A F, Westra S, Allan R P, Ban N, Barbero R, Berg P, Blenkinsop S and Do H X 2021 Anthropogenic intensification of short-duration rainfall extremes *Nat. Rev. Earth Environ.* **2** 107–22
Fujinami H, Yasunari T and Watanabe T 2016 Trend and interannual variation in summer precipitation in eastern Siberia in recent decades *Int. J. Climatol.* **36** 355–68
Grimm A M 2011 Interannual climate variability in South America: impacts on seasonal precipitation, extreme events, and possible effects of climate change *Stoch. Environ. Res. Risk Assess.* **25** 537–54
Ha K J, Moon S, Timmermann A and Kim D 2020 Future changes of summer monsoon characteristics and evaporative demand over Asia in CMIP6 simulations *Geophys. Res. Lett.* **47** e2020GL087492
Hodel F H and Fieberg J R 2021 Cylcop: an R package for circular-linear copulae with angular symmetry *bioRxiv Preprint* (https://doi.org/10.1101/2021.07.14.452253) (Accessed 1 September 2023)
Hodel F H and Fieberg J R 2022 Circular–linear copulae for animal movement data *Meth. Ecol. Evolut.* **13** 1001–13
IPCC 2021 Climate change 2021—the physical science basis: working group I contribution to the sixth assessment report of the intergovernmental panel on climate change *Masson-Delmotte* ed V P Zhai *et al* (Cambridge University Press)
Iturbide M *et al* 2020 An update of IPCC climate reference regions for subcontinental analysis of climate model data: definition and aggregated datasets *Earth Syst. Sci. Data* **12** 2959–70
Jiang Y, Zhou L, Roundy P E, Hua W and Raghavendra A 2021 Increasing influence of Indian Ocean dipole on precipitation over central equatorial Africa *Geophys. Res. Lett.* **48** e2020GL092370
Katzenberger A, Schewe J, Pongratz J and Levermann A 2021 Robust increase of Indian monsoon rainfall and its variability under future warming in CMIP6 models *Earth Syst. Dyn.* **12** 367–86
Kent C, Chadwick R and Rowell D P 2015 Understanding uncertainties in future projections of seasonal tropical precipitation *J. Clim.* **28** 4390–13
Khan S J, Deere D, Leusch F D, Humpage A, Jenkins M and Cunliffe D 2015 Extreme weather events: should drinking water quality management systems adapt to changing risk profiles? *Water Res.* **85** 124–36
Kim H and Villarini G 2024 higher emissions scenarios lead to more extreme flooding in the United States *Nat. Commun.* **15** 237
Kotz M, Levermann A and Wenz L 2022 The effect of rainfall changes on economic production *Nature* **601** 223–7
Lehmann J, Coumou D and Frieler K 2015 Increased record-breaking precipitation events under global warming *Clim. Change* **132** 501–15
Lei H, Ma Q, Chang Y, Gu Y, Wan S, Zhu Z and Feng G 2024 Multiscale interactions driving summer extreme precipitation in Central Asia *Geophys. Res. Lett.* **51** e2024GL108882
Li M and Ma Z 2018 Decadal changes in summer precipitation over arid northwest China and associated atmospheric circulations *Int. J. Climatol.* **38** 4496–508
Li X, Hu Q, Wang R, Zhang D and Zhang Q 2021 Influences of the timing of extreme precipitation on floods in Poyang Lake, China *Hydrol. Res.* **52** 26–42
Llasat M C, Del Moral A, Cortès M and Rigo T 2021 Convective precipitation trends in the Spanish Mediterranean region *Atmos. Res.* **257** 105581
Marelle L, Myhre G, Hodnebrog Ø, Sillmann J and Samset B H 2018 The changing seasonality of extreme daily precipitation *Geophys. Res. Lett.* **45** 11,352–60
Menon A, Levermann A, Schewe J, Lehmann J and Frieler K 2013 Consistent increase in Indian monsoon rainfall and its variability across CMIP-5 models *Earth Syst. Dyn.* **4** 287–300
Monerie P-A, Pohl B and Gaetani M 2021 The fast response of Sahel precipitation to climate change allows effective mitigation action *npj Clim. Atmos. Sci.* **4** 24
Nicholson S E 2018 The ITCZ and the seasonal cycle over equatorial Africa *Bull. Am. Meteorol. Soc.* **99** 337–48
Nissen K M and Ulbrich U 2017 Increasing frequencies and changing characteristics of heavy precipitation events threatening infrastructure in Europe under climate change *Nat. Hazards Earth Syst. Sci.* **17** 1177–90
Organization W H 2018 *The State of Food Security and Nutrition in the World 2018: Building Climate Resilience for Food Security and Nutrition* (Food & Agriculture Org)
Pewsey A, Neuhäuser M and Ruxton G D 2013 *Circular Statistics in R* (OUP Oxford)
Raleigh C and Kniveton D 2012 Come rain or shine: an analysis of conflict and climate variability in East Africa *J. Peace Res.* **49** 51–64
Rosenzweig C, Tubiello F N, Goldberg R, Mills E and Bloomfield J 2002 Increased crop damage in the US from excess precipitation under climate change *Glob. Environ. Change* **12** 197–202
Schär C *et al* 2016 Percentile indices for assessing changes in heavy precipitation events *Clim. Change* **137** 201–16
Seneviratne S I *et al* 2021 Weather and climate extreme events in a changing climate *The Physical Science Basis. Contribution of Working Group I to the Sixth Assessment Report of the Intergovernmental Panel on Climate Change* ed V Masson-Delmotte *et al* (Cambridge University Press) pp 1513–766
Seth A, Rauscher S A, Rojas M, Giannini A and Camargo S J 2011 Enhanced spring convective barrier for monsoons in a warmer world? A letter *Clim. Change* **104** 403–14
Song F, Leung L R, Lu J and Dong L 2018 Seasonally dependent responses of subtropical highs and tropical rainfall to anthropogenic warming *Nat. Clim. Change* **8** 787–92
Song F, Leung L R, Lu J, Zhou T and Huang P 2023 Advances in understanding the changes of tropical rainfall annual cycle: a review *Environ. Res. Clim.* **2** 042001
Song F, Lu J, Leung L R and Liu F 2020 Contrasting phase changes of precipitation annual cycle between land and ocean under global warming *Geophys. Res. Lett.* **47** e2020GL090327
Thackeray C W, Hall A, Norris J and Chen D 2022 Constraining the increased frequency of global precipitation extremes under warming *Nat. Clim. Change* **12** 441–8
Thomas K M, Charron D F, Waltner-Toews D, Schuster C, Maarouf A R and Holt J D 2006 A role of high impact

weather events in waterborne disease outbreaks in Canada, 1975–2001 *Int. J. Environ. Health Res.* **16** 167–80

Veatch W and Villarini G 2020 Modeling the seasonality of extreme coastal water levels with mixtures of circular probability density functions *Theor. Appl. Climatol.* **140** 1199–206

Veatch W and Villarini G 2022 Modeling riverine flood seasonality with mixtures of circular probability density functions *J. Hydrol.* **613** 128330

Wainwright C M, Black E and Allan R P 2021 Future changes in wet and dry season characteristics in CMIP5 and CMIP6 simulations *J. Hydrometeorol.* **22** 2339–57

Wasko C, Nathan R and Peel M C 2020 Changes in antecedent soil moisture modulate flood seasonality in a changing climate *Water Resour. Res.* **56** e2019WR026300

Weltzin J F *et al* 2003 Assessing the response of terrestrial ecosystems to potential changes in precipitation *BioScience* **53** 941–52

Westra S, Fowler H J, Evans J P, Alexander L V, Berg P, Johnson F, Kendon E J, Lenderink G and Roberts N 2014 Future changes to the intensity and frequency of short-duration extreme rainfall *Rev. Geophys.* **52** 522–55

Wu S-Y, Wu Y and Wen J 2019 Future changes in precipitation characteristics in China *Int. J. Climatol.* **39** 3558–73

Xu P, Wang L and Ming J 2022 Central Asian precipitation extremes affected by an intraseasonal planetary wave pattern *J. Clim.* **35** 2603–16

Zarrin A, Dadashi-Roudbari A and Hassani S 2021 Historical variability and future changes in seasonal extreme temperature over Iran *Theor. Appl. Climatol.* **146** 1227–48

Zeppel M, Wilks J V and Lewis J D 2014 Impacts of extreme precipitation and seasonal changes in precipitation on plants *Biogeosciences* **11** 3083–93

Zhang W and Villarini G 2017 Heavy precipitation is highly sensitive to the magnitude of future warming *Clim. Change* **145** 249–57